Postprint. Jingwen Wang, et al., Separation and Purification Technology 248 (2020) 117053.
https://doi.org/10.1016/j.seppur.2020.117053

Multilevel Screening of Ionic Liquid Absorbents for Simultaneous Removal of CO_2 and H_2S from Natural Gas

Jingwen Wang,[a] Zhen Song,[b,c,*] Hongye Cheng,[a] Lifang Chen,[a]

Liyuan Deng,[d] and Zhiwen Qi[a,*]

[a] *State Key Laboratory of Chemical Engineering, School of Chemical Engineering, East China University of Science and Technology, 130 Meilong Road, 200237, Shanghai, China*

[b] *Process Systems Engineering, Max Planck Institute for Dynamics of Complex Technical Systems, Sandtorstr. 1, D-39106 Magdeburg, Germany*

[c] *Process Systems Engineering, Otto-von-Guericke University Magdeburg, Universitätsplatz 2, D-39106 Magdeburg, Germany*

[d] *Department of Chemical Engineering, Norwegian University of Science and Technology, Sem Sælandsvei 4, 7491 Trondheim, Norway*

[*] *Corresponding authors:* songz@mpi-magdeburg.mpg.de (Z. S.); zwqi@ecust.edu.cn (Z. Q.)

ABSTRACT

For the selection of practically attractive ionic liquids (ILs) as absorbents for simultaneous CO_2 and H_2S removal from natural gas (NG), a multilevel screening method combining Henry′s law constant (*H*) and vapor-liquid equilibria (VLE) based prediction of thermodynamic properties, physical properties estimation, and process simulation is presented. To begin with, an *H*-based Absorption-Selectivity-Desorption index (*ASDI*) is employed to prescreen potential ILs that have promising target properties at infinite dilution condition. Following this, their simultaneous CO_2 and H_2S removal performances are further evaluated from the VLE of {IL + NG} systems at the specific composition of interest. After the thermodynamic screening, key physical properties of the obtained ILs are estimated by group contribution methods and the IL stability is assessed empirically to find out solvents suitable for practical application. Finally, continuous acidic gas removal processes based on the remaining ILs are

simulated and compared by Aspen Plus, thereby identifying the best ILs from the process point of view.

KEYWORDS: ionic liquid screening, simultaneous acidic gas removal, Henry′s law constant, vapor-liquid equilibria, process simulation

1. INTRODUCTION

As one of the most dominant global energy sources, natural gas (NG) has been increasingly utilized during the past decades [1,2]. However, the undesirable contaminants accompanying CH_4 in raw NG, that is, acidic gases CO_2 and H_2S will lead to severe problems such as toxicity, equipment corrosion, and decrease in calorific value of NG [3-6]. Therefore, the removal of CO_2 and H_2S from NG is of great significance from both economic and safety point of view [7-10]. So far, aqueous alkanolamines based chemical absorption and the Rectisol technology using cold methanol as physical absorbent have been widely applied in the chemical industry [11,12]. However, such processes suffer heavily from high energy consumption caused by solvent regeneration and the very low operating temperature [13], respectively. Therefore, searching competitive alternatives to alkanolamines and methanol is highly significant.

In the past decades, ionic liquids (ILs) have been extensively explored as gas absorbents due to their overwhelming merits over conventional organic solvents, such as negligible vapor pressure, high chemical/thermal stability, designable and tunable character [14,15]. Until now, the absorption behaviors of ILs for gases such as CO_2, H_2S, N_2, H_2, and C1 − C4 hydrocarbons have been continuously reported, which indicate the high potential of ILs as acidic gas absorbents [16-19]. However, as the gas-in-IL solubility varies remarkably from case to case, the selection of proper ILs is of

central importance to ensure a technically and economically feasible IL-based acidic gas removal process [20-22]. So far, most studies on IL-based gas absorption still focus on the experimental measurement of gas solubility in ILs [23,24], covering only a small proportion of IL candidates among the large quantity of possible cation-anion combinations. For instance, for this particular NG purification case, there are very limited data on the CH_4-in-IL solubility. To search more optimal IL solvents over a large space, the experimental approach is costly, time-consuming, and even unrealistic to explore the various IL possibilities. In this context, predictive thermodynamic models have been developed and applied for theoretical IL screening or design [15,16,21,25-31].

Among the predictive thermodynamic models, COSMO-based activity coefficient models (i.e., COSMO-RS and COSMO-SAC) merely require quantum-chemically derived molecular descriptors as inputs for the thermodynamic property prediction, and thus are widely used in IL selection for gas absorption tasks as well as other separation processes [15,29,30,32-35]. For example, Farahipour proposed a systematic screening methodology with COMSO-RS to screen ILs possessing both high absorption capacity and desorption property for CO_2 capture [35]. Very recently, our group further developed a COSMO-SAC based IL design method with an integrated mass-based Absorption-Selectivity-Desorption index (*ASDI*) as the design objective for CO_2 separation from flue gas (CO_2/N_2), syngas (CO_2/H_2) and sour gas (CO_2/H_2S) [34].

Despite the progress made, the above IL screening or design work as well as other similar studies only considered the single gas capture or the two-component mixture separation cases. To the best of our knowledge, the computational selection of ILs for simultaneous removal of CO_2 and H_2S has not been reported. Moreover, most previous studies on IL selection only relied on a simple and quick estimation of the

thermodynamic properties at the infinite dilution condition [26,34-36]. However, such screening may not lead to the optimal solvent for practical systems due to the neglect of real absorption conditions, that is, the multi-components and finite concentrations. In this regard, it is of high interest to evaluate the separation performances of IL candidates at the specific conditions of interest at the solvent screening stage [37,38].

In addition to the thermodynamic criteria, some fundamental physical properties, especially the melting point (T_m) and viscosity (η), as well as the IL stability, are important for determining the suitability of solvents as absorbents, and thus should also be taken into account during the IL screening [39,40]. Besides, it is always preferred that the optimal absorbent for an IL-based acidic gas removal task is finally identified based on the highest performance in the continuous process; whereas it is unrealistic to evaluate the process performances of a large number of ILs without a preliminary screening by thermodynamic and physical properties [18,41,42].

Taking account of the essential aspects mentioned above, this contribution combines the prediction of thermodynamic properties derived from Henry's law constant (H) and vapor-liquid equilibria (VLE) at the global compositions of interest, the estimation of physical properties, and the process simulation to screen suitable ILs as absorbents for simultaneous removal of CO_2 and H_2S from NG.

2. METHODS

The whole method for screening IL absorbents for simultaneous CO_2 and H_2S removal is structured in Figure 1, which consists of four steps:

Step 1: IL prescreening based on the H-derived *ASDI*. The H-based *ASDI* values of different cation-anion combinations towards the individual CO_2/CH_4 and H_2S/CH_4 separation tasks are calculated; the ILs with lower *ASDI* (corresponding to higher absorption performance) in both individual cases are preliminarily selected for further

consideration.

Step 2: ILs screening based on the VLE-derived *ASDI′*. The VLE of systems composed of the target NG mixture {CO_2 + H_2S + CH_4} and different prescreened ILs at the specific global composition are calculated and the corresponding *ASDI′* derived from the VLE results are compared in this step. The candidates presenting lower *ASDI′* for the two individual tasks (CO_2/CH_4 and H_2S/CH_4) are retained.

Step 3: ILs screening based on the physical properties and stability. The T_m and η of the prescreened candidates are estimated to further find out the ones with desired physical properties and the potential IL stability is assessed.

Step 4: ILs screening based on the process simulation. In this step, the IL candidates remained after the first three steps are evaluated in the continuous acidic gas absorption processes and compared with previously-reported benchmark ILs. The optimal process-based ILs are finally identified by comparing the process simulation results such as the required column height, solvent and energy consumptions.

In the following, more details on the multilevel screening method are elaborated.

2.1. *H*-based *ASDI* calculation

For gas absorption processes, the absorption capacity (*A*) and selectivity (*S*) as well as the desorption capacity (*D*) are all important performance indices from thermodynamic point of view, however, usually present contradictory dependencies on IL structures [14,35]. In the previous study [34], the *ASDI* has been demonstrated to be very suitable thermodynamic index for screening ILs as it can make a good trade-off among these three indices without giving constraints on each single index, and thus is employed as the performance index to evaluate the IL candidates. Considering this criterion is defined only for two-component gas mixture, the simultaneous removal of CO_2 and H_2S from CH_4 is first modeled by two individual tasks of CO_2/CH_4 and

H_2S/CH_4 separation. In this manner, in addition to output the most potential IL structure for this multi-component gas removal task, useful insights into (1) the effects of IL structure on the individual CO_2/CH_4 and H_2S/CH_4 separation and (2) the way to reach the trade-off for the simultaneous CO_2 and H_2S removal can be offered. For each task, the mass-based *ASDI* is calculated as:

$$ASDI = H_{i/\mathrm{IL}} \times \frac{1}{S_{i/\mathrm{CH_4}}} \times D \tag{1}$$

where *i* refers to the target gas componenet (CO_2, H_2S); *H*, *S* and *D* represent the mass-based Henry's law constant, selectivity towards CH_4, and desorption capacity of these two gases in ILs, respectively (see Eqs. (2) – (4)).

$$H_{i/\mathrm{IL}} = H^{\mathrm{mole}}{}_{i/\mathrm{IL}}(T) \times \frac{M_{\mathrm{IL}}}{M_i} \tag{2}$$

$$S_{i/\mathrm{CH_4}} = \frac{H^{\mathrm{mole}}{}_{\mathrm{CH_4/IL}}}{H^{\mathrm{mole}}{}_{i/\mathrm{IL}}} \times \frac{M_i}{M_{\mathrm{CH_4}}} \tag{3}$$

$$D = \frac{(H^{\mathrm{mole}}_{i/\mathrm{IL}})_{298.15K}}{(H^{\mathrm{mole}}_{i/\mathrm{IL}})_{328.15K}} \tag{4}$$

where M_{IL}, M_i, and M_{CH4} are the molecular weights of IL, component *i*, and CH_4, respectively; H^{mole} stands for the mole-based Henry's law constant, which is estimated as the product of the saturated vapor pressure (P_i^s) and infinite dilution activity coefficient (γ_i^∞).

$$H^{\mathrm{mole}}{}_{i/s}(T) = P_i^s \gamma_i^\infty \tag{5}$$

The Antoine equation is employed to calculate the P_i^s of involved gas components at different temperatures. For the γ_i^∞ calculation of NG components in ILs, the COSMO-SAC model is employed where the σ-profiles and V_{COSMO} of the involved cations and anions are obtained from the quantum mechanical calculations by the DMol^3 module

in the Accelrys Materials Studio 6.1 software package [43]. The detailed introduction on the activity coefficient prediction using COSMO-SAC can be found in previous literature [33,37,44].

2.2. VLE based *ASDI'* prediction

As the separation performance suggested from the thermodynamic properties at infinite dilution may differ from those at the practical condition [45], it is highly valuable to further evaluate the VLE performance of the ILs prescreened from *H*-based *ASDI*. Here, the raw NG is assumed as a mixture of {CO_2 + H_2S + CH_4} with a mass fraction of [0.15, 0.05, 0.80] [8]. The VLE of {IL + NG} at the specific global composition of 1:1 is calculated by COSMO-SAC as a flash problem to simulate the IL-involved acidic gas removal process; a VLE-derived criterion *ASDI'* is proposed to evaluate the practical absorption performance of ILs as defined in Eq. (6).

$$ASDI' = \frac{1}{\beta_i} \times \frac{1}{S'_{i/\mathrm{CH_4}}} \times D' \tag{6}$$

where the β_i, $S'_{i/\mathrm{CH_4}}$, D' are the distribution coefficient, selectivity, and desorption coefficient, respectively, which are calculated from the VLE results as follows.

$$\beta_i = \frac{m_i^L}{m_i^V} \tag{7}$$

$$S' = \frac{m_i^L}{m_i^V} / \frac{m_{\mathrm{CH_4}}^L}{m_{\mathrm{CH_4}}^V} \tag{8}$$

$$D' = \left(\frac{m_i^L}{m_i^V}\right)_{328.15K} / \left(\frac{m_i^L}{m_i^V}\right)_{298.15K} \tag{9}$$

In Eqs. (7) – (9), m_i and $m_{\mathrm{CH_4}}$ represent the mass fractions of the target components (CO_2, H_2S) and CH_4 in the VLE compositions; superscripts *L* and *V* denote the liquid and the gas phases, respectively.

2.3. Physical property estimation and stability assessment

To screen out ILs suitable for practical application, the physical properties of ILs are taken into account. For the estimation of T_m and η of the ILs, two group contribution (GC) models are employed, respectively (see Eqs. (10) and (11)).

$$T_m\left(K\right) = 288.7 + \sum_{j}^{N_g} n_j \Delta t_j \tag{10}$$

$$\ln \eta\left(cP\right) = 6.982 + \sum_{j}^{N_g} n_j a_j + \sum_{j}^{N_g} n_j b_j / T \tag{11}$$

where n_j is the occurrence of the group j in the IL; Δt_j is the contribution of group j to the melting point, and a_j and b_j are the contribution parameters of group j to the viscosity. Both the two above models are parametrized from a large number of experimental data and have been proven to be reliable prediction tools for estimating IL physical properties in IL selection [39,40].

Beyond the physical properties, the thermal and chemical stability of IL candidates are also highly significant in determining the suitability of ILs as solvent. However, as there are so far no generally applicable prediction methods for these two properties, it is inconvenient to analyze such stability issues of a large number of ILs in the early screening stage. In this work, the potential thermal and chemical stability for the top candidates obtained after the prescreening by thermodynamic and physical properties are assessed from the empirical point of view.

2.4. Aspen Plus-based process simulation and evaluation

In this work, Aspen Plus V8.4 is employed to simulate the continuous acidic gas removal process with the rate-based methods, where the ILs retained after the first three steps and three benchmark IL absorbents reported in recent literature are compared [8,10,46]. The flowsheet of the IL-based process is shown in Figure 2, for which the

absorber and flash tanks are modeled by the *RadFrac* block and *Flash* block, respectively. The NG gas stream to be purified enters from the bottom of the absorber, contacting the IL stream counter-currently; the purified gas is then released from the top stream and the acidic gas-rich solvent flows into the IL regeneration units Flash-1 and Flash-2 successively. In order to reduce the CH_4 loss, the outlet stream from the top of Flash-1 is pressurized in the compressor and mixed with the feed gas before entering the absorber again while the bottom stream flows into the second flash tank to regenerate IL solvents. Finally, the absorbed CO_2 and H_2S is gathered after two single-stage flash process at the top of Flash-2 and the lean solvent is cooled and pumped for reuse. In this work, a Flexiring random packed (0.625in.) absorber is employed with the fractional capacity and equilibrium stage fixed as 62% and 10, respectively [46-49]. For each IL-based process, 1,000 $kg \cdot h^{-1}$ NG mixture with the same initial compositions as in the above VLE calculation is fed to the absorber as the feed stream. The main operating conditions of the absorber (i.e., the column height, absorption pressure and IL flow rate) and of the regeneration units (i.e., the operating temperature and pressure of Flash-1 and Flash-2) are roughly optimized to obtain high purity and recovery of CH_4, high removal of CO_2 and H_2S as well as high regenerated IL purity.

Since ILs have not been included in the component databanks in Aspen Plus, they are defined as pseudo-components by specifying their molecular weight (M), density (ρ), normal boiling temperature (T_b), viscosity and critical properties (T_c, P_c, V_c, ω). In this work, the required ρ, T_b, T_c, P_c, V_c, ω for the involved ILs are estimated by the fragment contribution - corresponding states (FC-CS) method reported by Huang et al [47], while the viscosity-to-temperature dependence of the ILs is specified through an Arrhenius type equation. As for the thermodynamic model, the COSMO-SAC method implemented in Aspen Plus is adopted with six parameters for each component, that is,

the CSACVL (V_{COSMO}) and SGPRF1 to SGPRF5 (σ-profiles) [48,49].

3. RESULTS AND DISCUSSION

3.1. Prescreening of ILs based on the *H*-derived *ASDI*

In this work, to screen out potential IL absorbents over a large feasible space, 1643 ILs are included in the initial database by combining 53 cations and 31 anions commonly seen in previous IL studies (the detailed structures of the involved cations and anions are shown in Table S1, Supporting Information). The *H*-based *ASDI* of these ILs for CO_2/CH_4 and H_2S/CH_4 are calculated and depicted in Figure 3 with the detailed data (*H*, *S*, *D* and *ASDI*) given in Table S2 – S9 (Supporting Information), respectively.

From Figure 3, the *ASDI* of the involved ILs varies in a large range for the two individual cases (10^{-2} – 10^{3} for CO_2/CH_4, 10^{-6} – 1 for H_2S/CH_4), highlighting the great importance of searching suitable cation-anion combinations for the CO_2 and H_2S removal process. Moreover, it can be found that anions play a more important role on the *ASDI* in comparison to the cations for both the CO_2/CH_4 and H_2S/CH_4 separations, which is consistent with the previous experimental and computational findings [24,34,35,50]. However, different types of ILs excel in the *ASDI* for these two individual separations, which may be attributed to the different interaction mechanisms of ILs for CO_2 and H_2S [15]. To be specific, ILs comprising phosphate ($[H_2PO_4]^-$, $[eFAP]^-$, $[DEP]^-$, $[DBP]^-$, $[DMP]^-$, $[bFAP]^-$), sulphate ($[MeSO_4]^-$, $[OcSO_4]^-$, $[DeOSO_4]^-$, $[EtSO_4]^-$, $[HSO_4]^-$) and ethylsulfonyl ($[Tf_2N]^-$, $[BETI]^-$) anions are favorable for the separation of CO_2 from CH_4 (corresponding to low *ASDI* values, see Figure 3a); whereas $[Cl]^-$, $[Br]^-$, $[For]^-$, $[Ac]^-$, $[SCN]^-$ and $[DCA]^-$-based ILs are superior for the H_2S/CH_4 separation as shown in Figure 3b.

From above, the optimal ILs for the CO_2 capture are not the best for the H_2S removal, and vice versa. To balance the separation performances of ILs for

simultaneous CO_2 and H_2S absorption, the ILs having the top 40% lowest *ASD*I values for both the individual CO_2/CH_4 and H_2S/CH_4 separations are prescreened. Consequently, 29 IL candidates survived in this step, which are based on five type of anions namely $[H_2PO_4]^-$, $[HSO_4]^-$, $[MeSO_4]^-$, $[EtSO_4]^-$, and $[MeSO_4]^-$ (see Table S10, Supporting Information).

3.2. Screening of ILs based on VLE-derived *ASDI'*

Before evaluating the VLE-based separation performances of the pre-screened candidates at practical condition, the prediction reliability of COSMO-SAC should be evaluated. This method has been demonstrated to be able to reliably predict the binary VLE of $\{CO_2/H_2S/CH_4 + IL\}$ as well as the Henry's law constants of various gases (e.g., CO_2, N_2, H_2, H_2S and $C_1 - C_4$) in ILs [29,34]. Here, only the prediction performance of COSMO-SAC for the VLE prediction of {gas mixtures + IL} systems involving NG components and ILs is further evaluated. For this purpose, the VLE data of four $\{CO_2 + H_2S + IL\}$, one $\{CO_2 + SO_2 + IL\}$, one $\{CO_2 + CH_4 + IL\}$, and one $\{CO_2 + O_2 + IL\}$ systems are calculated and compared to the experimental data (see the detailed data in Table S11, Supporting Information) [23,51-55]. Figures 4a and 4b illustrate the comparison of experimental and calculated VLE with two representative systems, i.e., $\{CO_2 + H_2S + [BMIM][MeSO_4]\}$ and $\{CO_2 + SO_2 + [HMIM][Tf_2N]\}$. As seen, the calculated *y-x* trend agrees well with the experimental result from both qualitative and quantitative point of view with the root mean square deviations (*RMSD*s) of 0.0225 and 0.0352, respectively. For the seven studied ternary systems, the average *RMSD* is 0.0515. Combining with the other validations in previous literature, the COSMO-SAC model could be reliably used for the following IL screening.

After the validation of COSMO-SAC, the VLE of the {IL + NG} systems based on the prescreened ILs in the first step are calculated at the specific global concentration

of interest and their VLE-derived *ASDI′* towards the CO_2 and H_2S removal tasks are compared to the *H*-based *ASDI* in Figure 5. The prescreened ILs are arranged in the increasing order of their *H*-based *ASDI* on the *x* axis for the convenience of comparison. However, no clear ranking of their VLE-derived *ASDI′* is found correspondingly. The notably different tendencies of the *H*-based *ASDI* and VLE-derived *ASDI′* clearly demonstrate the differences in separation performances of ILs estimated at infinite dilution and practical condition. Both the multi-component character and the practical concentration could be potential reasons responsible for such a difference, manifesting the necessity of the further screening of IL absorbents based on VLE.

From the VLE-derived *ASDI′* for CO_2/CH_4 and H_2S/CH_4 separation in Figure 6, one can note that the *ASDI′* values of the 29 ILs for H_2S/CH_4 are obviously lower than those for CO_2/CH_4 (0.2218 – 6.4450 versus 1.0055 – 83.9405), demonstrating the easier removal of H_2S over CO_2 from NG. Moreover, the *ASDI′* of ILs for the H_2S/CH_4 separation task of $[H_2PO_4]^-$, $[HSO_4]^-$, $[MeSO_4]^-$, $[EtSO_4]^-$ and $[MeSO_4]^-$-based ILs are at a similar level, which are 0.2218 – 1.3719, 1.2524 – 8.4548, 0.5357 – 6.4450, 0.9647 and 0.9342 – 3.0919, respectively; in contrast, the *ASDI′* of the $[H_2PO_4]^-$-based ILs (1.0055 – 3.7255) for CO_2/CH_4 separation are notably lower compared to those of other four types of ILs (12.4773 – 36.2960, 31.5246 – 83.9405, 48.7916, 32.7698 – 65.8442 for $[HSO_4]^-$, $[MeSO_4]^-$, $[EtSO_4]^-$ and $[MeSO_4]^-$-based IL, respectively). As a result, the ILs closest to the origin point are all the $[H_2PO_4]^-$ based ones (as marked in Figure 6). Therefore, the $[H_2PO_4]^-$-based ILs namely $[BMPYO][H_2PO_4]$, $[BeMPYO][H_2PO_4]$, $[BnMMIM][H_2PO_4]$, $[PMMIM][H_2PO_4]$, $[DePYO][H_2PO_4]$, and $[EMIM][H_2PO_4]$ are

screened out in this step.

3.3. Screening of ILs based on the physical properties and stability

To ensure that the selected ILs could act as liquid absorbents under room temperature and have relatively low viscosity, the upper bound of T_m and η are set to be 298.15 K and 100 cP, respectively. The physical properties of the six $[H_2PO_4]^-$-based ILs screened by thermodynamic criteria are estimated by the GC models and listed in Table S12 (Supporting Information). As seen, four ILs meeting such physical property constraints, i.e., [BeMPYO][H_2PO_4], [PMMIM][H_2PO_4], [DePYO][H_2PO_4] and [EMIM][H_2PO_4], are retained.

In previous literature [56], $[H_2PO_4]^-$-based ILs with pyridinium as cation are experimentally determined to have decomposition temperature around 450 K. As the anion type plays the major role in the thermal stability of ILs, a similar thermal stability of the prescreened $[H_2PO_4]^-$-based ILs could be indicated. Moreover, as the conjugated anion of the mediate strong acid H_3PO_4, $[H_2PO_4]^-$ is unable to obtain proton from the cation and thus the cation-anion combination should be chemically stable [57]. Besides, to the best of our knowledge, chemical absorption is mainly observed in the cases of (a) CO_2/H_2S + basic ILs (i.e., NH_2-functionalized ILs) or weak acidic anion based ILs (e.g., $[Gly]^-$, $[Ac]^-$, $[Pro]^-$, $[Lev]^-$) and (b) H_2S + high oxidizing type of ILs (e.g., $[FeCl_4]^-$-based ILs) [58,59]. In this sense, the absorption of CO_2 and H_2S by the prescreened $[H_2PO_4]^-$-type ILs should be physically based and thus the ILs could remain stable during the absorption processes. Taking account of all these aspects, the four $[H_2PO_4]^-$-based ILs possess high practical suitability as absorbents for the studied task.

3.4. Screening of ILs based on process simulation

In this section, the four ILs obtained after the first three steps are evaluated in the continuous acidic gas removal process using the rate-based modes in Aspen Plus, and

compared with three benchmark ILs previously reported in literature ([BMIM][$MeSO_4$], [BMIM][PF_6] and [BMIM][TCM]) [8,10,46]. It is worth mentioning that these three benchmark ILs are also included in our initial database but are discarded in the thermodynamic screening step. As described previously, the required properties of all the involved absorbents are calculated and listed in Table S13 (Supporting Information). In the following, the process optimization procedure is exemplified by the [DePYO][H_2PO_4]-based process.

To begin with, the column height is optimized to minimize the kinetic effect by performing a sensitivity analysis. As plotted in Figures 7a and 7b, the purity and recovery of CH_4 as well as the removal of CO_2 and H_2S ascend with the increasing column height below 14 m and afterwards keep almost constant. Hence, the column height of the absorber is determined as 14 m. Afterward, the pressure in the absorber and IL flow rate are optimized. As depicted in Figure 8a – 8b, with the pressure in the absorber increasing from 1 bar to 6 bar, the purity and recovery of CH_4 rise from 83.59 wt% to 98.00 wt% and from 96.53% to 97.93%, respectively; the removal of CO_2 and H_2S grow from 22.32% to 91.77% and from 29.90% to 92.76% accordingly. After that, all these process objectives only increase slightly, and thus the absorption pressure is set to be 6 bar. From Figures 9a and 9b, it is clear that the CH_4 purity and the removal of CO_2 and H_2S follow almost the same trends against the IL flow rate, which is, however, reverse with that of the CH_4 recovery. Specifically, with the IL flow rate increasing from 10,000 to 23,000 $kg \cdot h^{-1}$, the CH_4 purity and the removal of CO_2 and H_2S increases dramatically and the CH_4 recovery decreases smoothly. However, further increasing the IL flow rate only enhances the CH_4 purity and the removal of CO_2 and H_2S trivially while reduces the CH_4 recovery notably. Therefore, the optimal IL flow rate is determined to be 23,000 $kg \cdot h^{-1}$.

As the key parameters for the IL regeneration units, the temperature and pressure of the flash tanks are studied. As seen in Figures 10a – 10b, the CH_4 recovery almost declines linearly with increasing the pressure in the range of 1 bar – 6 bar at different temperatures whereas the CH_4 purity stays very closely in the pressure range with the temperature lower than 353.15 K. Therefore, the Flash-1 is operated at the atmosphere pressure (1 bar) to ensure both high CH_4 recovery and purity. At the fixed pressure, the CH_4 purity goes down sharply with increasing the temperature from 353.15 K (97.79 wt%) to 383.15 K (91.99 wt%) while the CH_4 recovery changes mildly within a high level (97.91% – 99.32%). As a consequence, the temperature of Flash-1 is determined to be 353.15 K. As seen from Figures 11a – 11c, the temperature and pressure in Flash-2 mainly affect the CH_4 purity (in the range of 80.00 wt% – 99.14 wt%) with the CH_4 recovery and the regenerated IL mass purity remain always at a high level above 97.50%. Thus, the parameters of Flash-2 are mainly determined based on the CH_4 purity. As demonstrated in Figure 11a, higher temperature and lower pressure are preferred for high CH_4 purity in the product; however, such conditions will inevitably result in higher energy consumption for the compressor and heater. Taking account of above aspects, the operating temperature and pressure are set at 373.15 K and 0.3 bar, respectively, as the CH_4 purity and recovery go up more steadily after that.

Following the above process optimization procedure, the final operating conditions as well as the main simulation results of the acidic gas removal processes based on the four screened candidates and three literature-reported ILs are summarized in Table 1. As seen, when achieving both high CH_4 purity and recovery in the simultaneous acidic gas removal task, the CO_2 and H_2S removal ratios based on the four ILs screened in this work are at a similar level, i.e., 90%, indicating a good trade-off between their CO_2 and H_2S absorption performances; in comparison, based on the

benchmark ILs [BMIM][$MeSO_4$], [BMIM][PF_6] and [BMIM][TCM], the continuous process can only reach an obviously lower removal ratio of CO_2 than H_2S, which implies the unbalanced absorption performances of these two acidic gases. Moreover, in comparison to the four prescreened $[H_2PO_4]^-$-type ILs, the required column height, IL amounts and energy consumptions based on the [BMIM][$MeSO_4$] and [BMIM][PF_6] are almost 5 – 7, 4 – 10 and 2 times higher, respectively; although the required column height based on [BMIM][TCM] is slightly lower (10 m vs. 12 – 14 m), the solvent and energy consumptions in this case are almost five times larger. All the above comparisons demonstrate the higher potential of the selected ILs for the acidic gas removal from natural gas and thus suggest the practicality of the IL screening method proposed in this work. Finally, by comparing the required column height with IL and energy consumptions in the continuous processes, [BeMPYO][H_2PO_4] and [EMIM][H_2PO_4] are identified as the best two absorbents for the simultaneous removal of CO_2 and H_2S from NG.

4. CONCLUSION

This work presents a multilevel screening of IL absorbents for the simultaneous removal of CO_2 and H_2S from raw natural gas (NG). From 1643 cation-anion combinations, 29 ILs are first prescreened out with top 40% lowest *H*-based Absorption-Selectivity-Desorption index (*ASDI*) for both the individual CO_2/CH_4 and H_2S/CH_4 separations. The simultaneous CO_2 and H_2S removal performances of these 29 ILs are further evaluated by calculating the vapor-liquid equilibria (VLE) of {IL + NG} at the specific global composition of interest, where $[H_2PO_4]^-$-based ILs are screened from the VLE-based *ASDI'* point of view. Subsequently, four ILs namely [BeMPYO][H_2PO_4], [PMMIM][H_2PO_4], [DePYO][H_2PO_4] and [EMIM][H_2PO_4] are found to satisfy the melting point and viscosity constraints imposed for practical

application with potential good thermal and chemical stability. Through the process simulation of continuous acidic gas absorption, these four ILs are all found to have notably higher process performances than the three benchmark ILs, among which [BeMPYO][H_2PO_4] and [EMIM][H_2PO_4] are identified as the best two absorbents. Beyond the highlighted task of simultaneous acid gas removal from NG, the proposed method could be easily extended to screen practically attractive IL absorbents for other gas separation tasks involving either single or multiple target components.

SUPPORTING INFORMATION

The Supporting information associated with this article can be found online at ****.

ACKNOWLEDGEMENT

The financial support from National Natural Science Foundation of China (21576081, 21776074 and 2181101120) is greatly acknowledged.

REFERENCES

(1) J. Abdulsalam, J. Mulopo, M.K. Amosa, S. Bada, R. Falcon, B.O. Oboirien, Towards a cleaner natural gas production: recent developments on purification technologies, Sep. Purif. Technol. 54 (2019) 2461-2497.

(2) M.A. Qyyum, Y.D. Chaniago, W. Ali, K. Qadeer, M. Lee, Coal to clean energy: Energy-efficient single-loop mixed-refrigerant-based schemes for the liquefaction of synthetic natural gas, J. Cleaner Prod. 211 (2019) 574-589.

(3) R.W. Baker, K. Lokhandwala, Natural gas processing with membranes: An overview, Ind. Eng. Chem. Res. 47 (2008) 2109-2121.

(4) K. Qadeer, M.A. Qyyum, M. Lee, Krill-Herd-Based Investigation for Energy Saving Opportunities in Offshore Liquefied Natural Gas Processes, Ind. Eng. Chem. Res. 57 (2018) 14162-14172.

(5) R. Santiago, J. Lemus, A.X. Outomuro, J. Bedia, J. Palomar, Assessment of ionic liquids as H_2S physical absorbents by thermodynamic and kinetic analysis based on process simulation, Sep. Purif. Technol. 233 (2020) DOI: 10.1016/j.seppur.2019.116050.

(6) S. Sridhar, B. Smitha, T.M. Aminabhavi, Separation of carbon dioxide from natural gas mixtures through polymeric membranes - A review, Sep. Purif. Rev. 36 (2007) 113-174.

(7) A.I. Akhmetshina, N.R. Yanbikov, A.A. Atlaskin, M.M. Trubyanov, A. Mechergui, K.V. Otvagina, E.N. Razov, A.E. Mochalova, I.V. Vorotyntsev, Acidic Gases Separation from Gas Mixtures on the Supported Ionic Liquid Membranes Providing the Facilitated and Solution-Diffusion Transport Mechanisms, Membr. 9 (2019) DOI:10.3390/membranes9010009.

(8) A. Kazmi, J. Haider, M.A. Qyyum, S. Saeed, M.R. Kazmi, M. Lee, Heating load depreciation in the solvent-regeneration step of absorption-based acid gas removal using an ionic liquid with an imidazolium-based cation, Int. J. Greenhouse Gas Control 87 (2019) 89-99.

(9) Y.L. Wang, X.B. Liu, A. Kraslawski, J. Gao, P.Z. Cui, A novel process design for CO_2 capture and H_2S removal from the syngas using ionic liquid, J. Cleaner Prod. 213 (2019) 480-490.

(10) X. Zhang, Z. Tu, H. Li, K. Huang, X. Hu, Y. Wu, D.R. MacFarlane, Selective separation of H_2S and CO_2 from CH_4 by supported ionic liquid membranes, J. Membr. Sci. 543 (2017) 282-287.

(11) W.H. Chen, S.M. Chen, C.I. Hung, Carbon dioxide capture by single droplet using Selexol, Rectisol and water as absorbents: A theoretical approach, Appl. Energy 111 (2013) 731-741.

(12) Z. Ziobrowski, R. Krupiczka, A. Rotkegel, Carbon dioxide absorption in a packed column using imidazolium based ionic liquids and MEA solution, Int. J. Greenhouse Gas Control 47 (2016) 8-16.

(13) S. Mukherjee, P. Kumar, A. Hosseini, A.D. Yang, P. Fennell, Comparative

Assessment of Gasification Based Coal Power Plants with Various CO_2 Capture Technologies Producing Electricity and Hydrogen, Energy Fuels 28 (2014) 1028-1040.

(14) M.B. Shiflett, A.D. Shiflett, A. Yokozeki, Separation of tetrafluoroethylene and carbon dioxide using ionic liquids, Sep. Purif. Technol. 79 (2011) 357-364.

(15) Y.S. Zhao, R. Gani, R.M. Afzal, X.P. Zhang, S.J. Zhang, Ionic Liquids for Absorption and Separation of Gases: An Extensive Database and a Systematic Screening Method, AIChE J. 63 (2017) 1353-1367.

(16) M. Althuluth, M.C. Kroon, C.J. Peters, Solubility of Methane in the Ionic Liquid 1-Ethyl-3-methylimidazolium Tris(pentafluoroethyl)trifluorophosphate, Ind. Eng. Chem. Res. 51 (2012) 16709-16712.

(17) B. Li, Y.F. Chen, Z.H. Yang, X.Y. Ji, X.H. Lu, Thermodynamic study on carbon dioxide absorption in aqueous solutions of choline-based amino acid ionic liquids, Sep. Purif. Technol. 214 (2019) 128-138.

(18) X.Y. Liu, Y. Huang, Y.S. Zhao, R. Gani, X.P. Zhang, S.J. Zhang, Ionic Liquid Design and Process Simulation for Decarbonization of Shale Gas, Ind. Eng. Chem. Res. 55 (2016) 5931-5944.

(19) M. Ramdin, S.P. Balaji, J.M. Vicent-Luna, J.J. Gutierrez-Sevillano, S. Calero, T.W. de Loos, T.J.H. Vlugt, Solubility of the Precombustion Gases CO_2, CH_4, CO, H_2, N_2, and H_2S in the Ionic Liquid [bmim][Tf_2N] from Monte Carlo Simulations, J. Phys. Chem. C 118 (2014) 23599-23604.

(20) H. Chao, Z. Song, H.Y. Cheng, L.F. Chen, Z.W. Qi, Computer-aided design and process evaluation of ionic liquids for n-hexane-methylcyclopentane extractive distillation, Sep. Purif. Technol. 196 (2018) 157-165.

(21) Z. Song, X. Hu, Y. Zhou, T. Zhou, Z. Qi, K. Sundmacher, Rational design of double salt ionic liquids as extraction solvents: Separation of thiophene/n-octane as example, AIChE J. 65 (2019) DOI: 10.1002/aic.16625.

(22) Z. Song, X. Li, H. Chao, F. Mo, T. Zhou, H. Cheng, L. Chen, Z. Qi, Computer-aided ionic liquid design for alkane/cycloalkane extractive distillation process,

Green Energy Environ. 4 (2019) 154-165.

(23) M.B. Shiflett, A.M.S. Niehaus, A. Yokozeki, Separation of CO_2 and H_2S Using Room-Temperature Ionic Liquid [bmim][$MeSO_4$], J. Chem. Eng. Data 55 (2010) 4785-4793.

(24) Y.Y. Zhang, X.Y. Ji, Y.J. Xie, X.H. Lu, Screening of conventional ionic liquids for carbon dioxide capture and separation, Appl. Energy 162 (2016) 1160-1170.

(25) P. Matheswaran, C.D. Wilfred, K.A. Kurnia, A. Ramli, Overview of Activity Coefficient of Thiophene at Infinite Dilution in Ionic Liquids and their Modeling Using COSMO-RS, Ind. Eng. Chem. Res. 55 (2016) 788-797.

(26) Z.G Lei, C.N Dai, W. Wang, B.H Chen, UNIFAC model for ionic liquid-CO_2 systems, AIChE J. 60 (2014) 716-729.

(27) Z.G. Lei, C.N. Dai, Q.A. Yang, J.Q. Zhu, B.H. Chen, UNIFAC Model for Ionic Liquid-CO (H_2) Systems: An Experimental and Modeling Study on Gas Solubility, AIChE J. 60 (2014) 4222-4231.

(28) L.Y. Garcia-Chavez, A.J. Hermans, B. Schuur, A.B. de Haan, COSMO-RS assisted solvent screening for liquid-liquid extraction of mono ethylene glycol from aqueous streams, Sep. Purif. Technol. 97 (2012) 2-10.

(29) B.S. Lee, S.T. Lin, Screening of ionic liquids for CO_2 capture using the COSMO-SAC model, Chem. Eng. Sci. 121 (2015) 157-168.

(30) C.D.Wilfred, Z. Man, Z.P. Chan, Predicting methods for sulfur removal from model oils using COSMO-RS and partition coefficient, Chem. Eng. Sci. 102 (2013) 373-377.

(31) Z. Song, C. Zhang, Z. Qi, T. Zhou, K. Sundmacher, Computer-aided design of ionic liquids as solvents for extractive desulfurization, AIChE J. 64 (2018) 1013-1025.

(32) J.P. Gutierrez, G.W. Meindersma, A.B. de Haan, COSMO-RS-Based Ionic-Liquid Selection for Extractive Distillation Processes, Ind. Eng. Chem. Res. 51 (2012) 11518-11529.

(33) J.N. Zhang, L. Qin, D.L. Peng, T. Zhou, H.Y. Cheng, L.F. Chen, Z.W. Qi,

COSMO-descriptor based computer-aided ionic liquid design for separation processes Part II: Task-specific design for extraction processes, Chem. Eng. Sci. 162 (2017) 364-374.

(34) J.W. Wang, Z. Song, H.Y. Cheng, L.F. Chen, L.Y. Deng, Z.W. Qi, Computer-Aided Design of Ionic Liquids as Absorbent for Gas Separation Exemplified by CO_2 Capture Cases, ACS Sustainable Chem. Eng. 6 (2018) 12025-12035.

(35) R. Farahipour, A. Mehrkesh, A.T. Karunanithi, A systematic screening methodology towards exploration of ionic liquids for CO_2 capture processes, Chem. Eng. Sci. 145 (2016) 126-132.

(36) D.C. Weis, D.R. MacFarlane, Computer-Aided Molecular Design of Ionic Liquids: An Overview, Aust. J. Chem. 65 (2012) 1478-1486.

(37) S.T. Lin, S.I. Sandler, A priori phase equilibrium prediction from a segment contribution solvation model, Ind. Eng. Chem. Res. 41 (2002) 899-913.

(38) A.R. Ferreira, M.G. Freire, J.C. Ribeiro, F.M. Lopes, J.G. Crespo, J.A.P. Coutinho, Ionic liquids for thiols desulfurization: Experimental liquid-liquid equilibrium and COSMO-RS description, Fuel 128 (2014) 314-329.

(39) J.A. Lazzus, A group contribution method to predict the melting point of ionic liquids, Fluid Phase Equilib. 313 (2012) 1-6.

(40) J.A. Lazzús, G. Pulgar-Villarroel, A group contribution method to estimate the viscosity of ionic liquids at different temperatures, J. Mol. Liq. 209 (2015) 161-168.

(41) R. Santiago, J. Bedia, D. Moreno, C. Moya, J. de Riva, M. Larriba, J. Palomar, Acetylene absorption by ionic liquids: A multiscale analysis based on molecular and process simulation, Sep. Purif. Technol. 204 (2018) 38-48.

(42) J. de Riva, V. Ferro, C. Moya, M.A. Stadtherr, J.F. Brennecke, J. Palomar, Aspen Plus supported analysis of the post-combustion CO_2 capture by chemical absorption using the [P-2228][CNPyr] and [P-66614][CNPyr] AHA Ionic Liquids, Int. J. Greenhouse Gas Control 78 (2018) 94-102.

(43) B. Delley, An all-electron numerical method for solving the local density

functional for polyatomic molecules. J. Chem. Phys. 92 (1990) 508-517.

(44) E. Mullins, Y.A. Liu, A. Ghaderi, S.D. Fast, Sigma Profile Database for Predicting Solid Solubility in Pure and Mixed Solvent Mixtures for Organic Pharmacological Compounds with COSMO-Based Thermodynamic Methods, Ind. Eng. Chem. Res. 47 (2008) 1707-1725.

(45) Z. Song, T. Zhou, Z. Qi, K. Sundmacher, Systematic Method for Screening Ionic Liquids as Extraction Solvents Exemplified by an Extractive Desulfurization Process, ACS Sustainable Chem. Eng. 5 (2017) 3382-3389.

(46) J. Palomar, M. Larriba, J. Lemus, D. Moreno, R. Santiago, C. Moya, J. de Riva, G. Pedrosa, Demonstrating the key role of kinetics over thermodynamics in the selection of ionic liquids for CO_2 physical absorption, Sep. Purif. Technol. 213 (2019) 578-586.

(47) Y. Huang, H. Dong, X. Zhang, C. Li, S. Zhang, A new fragment contribution-corresponding states method for physicochemical properties prediction of ionic liquids, AIChE J. 59 (2013) 1348-1359.

(48) J. de Riva, J. Suarez-Reyes, D. Moreno, I. Díaz, V. Ferro, J. Palomar, Ionic liquids for post-combustion CO_2 capture by physical absorption: Thermodynamic, kinetic and process analysis, J. Greenhouse Gas Control 61 (2017) 61-70.

(49) J. Bedia, E. Ruiz, J. de Riva, V.R. Ferro, J. Palomar, J.J. Rodriguez, Optimized ionic liquids for toluene absorption, AIChE J. 59 (2013) 1648-1656.

(50) S. Zeng, X. Zhang, L. Bai, X. Zhang, H. Wang, J. Wang, D. Bao, M. Li, X. Liu, S. Zhang, Ionic-Liquid-Based CO_2 Capture Systems: Structure, Interaction and Process, Chem. Rev. 117 (2017) 9625-9673.

(51) M. Safavi, C. Ghotbi, V. Taghikhani, A.H. Jalili, A. Mehdizadeh, Study of the solubility of CO_2, H_2S and their mixture in the ionic liquid 1-octyl-3-methylimidazolium hexafluorophosphate: Experimental and modelling, J. Chem. Thermodyn. 65 (2013) 220-232.

(52) A.H. Jalili, M. Safavi, C. Ghotbi, A. Mehdizadeh, M. Hosseini-Jenab, V. Taghikhani, Solubility of CO_2, H_2S, and their mixture in the ionic liquid 1-octyl-

3-methylimidazolium bis(trifluoromethyl)sulfonylimide, J Phys. Chem. B 116 (2012) 2758-2774.

(53) M.B. Shiflett, A. Yokozeki, Separation of CO_2 and H_2S using room-temperature ionic liquid [bmim][PF_6], Fluid Phase Equilib. 294 (2010) 105-113.

(54) A. Yokozeki, M.B. Shiflett, Separation of Carbon Dioxide and Sulfur Dioxide Gases Using Room-Temperature Ionic Liquid [hmim][Tf_2N], Energy Fuels 23 (2009) 4701-4708.

(55) D.G. Hert, J.L. Anderson, S.N. Aki, J.F. Brennecke, Enhancement of oxygen and methane solubility in 1-hexyl-3-methylimidazolium bis(trifluoromethylsulfonyl) imide using carbon dioxide, Chem. Commun. (2005) 2603-2605.

(56) Y.Y. Cao, T.C. Mu, Comprehensive Investigation on the Thermal Stability of 66 Ionic Liquids by Thermogravimetric Analysis, Ind. Eng. Chem. Res. 53 (2014), 8651-8664.

(57) M. Fèvre, J. Pinaud, A. Leteneur, Y. Gnanou, J. Vignolle, D. Taton, Imidazol(in)ium Hydrogen Carbonates as a Genuine Source of N-Heterocyclic Carbenes (NHCs): Applications to the Facile Preparation of NHC Metal Complexes and to NHC-Organocatalyzed Molecular and Macromolecular Syntheses, J. Am. Chem. Soc. 134 (2012), 6776-6784.

(58) A. Yokozeki, M.B. Shiflett, C.P. Junk, L.M. Grieco, T. Foo, Physical and Chemical Absorptions of Carbon Dioxide in Room-Temperature Ionic Liquids, J. Phys. Chem. B 112 (2008), 16654-16663.

(59) J.H. Wang, W.D. Zhang, Oxidative Absorption of Hydrogen Sulfide by Iron-Containing Ionic Liquids, Energy Fuels 28 (2014), 5930-5935.

Table 1 Main results from the simulation of the continuous acidic gas removal processes using different ILs.

ILs		[DePYO][H_2PO_4]	[BeMPYO][H_2PO_4]	[PMMIM][H_2PO_4]	[EMIM][H_2PO_4]	[BMIM][$MeSO_4$]	[BMIM][PF_6]	[BMIM][TCM]
Operating conditions	Column height (m)	14	13	13	12	22	24	10
	Absorber pressure (bar)	6	6	6	6	6	6	6
	IL flowrate ($kg \cdot h^{-1}$)	23000	22000	23000	24000	124000	162000	106000
	Flash-1 temperature (K)	353.15	343.15	353.15	353.15	298.15	298.15	298.15
	Flash-1 pressure (bar)	1	1	1	1	1.2	1.8	1.2
	Flash-2 temperature (K)	373.15	383.15	373.15	373.15	423.15	373.15	383.15
	Flash-2 pressure(bar)	0.3	0.4	0.3	0.3	0.3	0.3	0.3
CH_4 purity (wt%)		97.47	97.36	97.21	97.52	97.01	96.86	97.26
CH_4 recovery (%)		98.76	97.22	97.92	95.37	96.85	95.71	97.78
CO_2 fraction in product (wt%)		2.04	2.01	2.07	1.96	2.78	2.67	2.47
H_2S fraction in product (wt%)		0.48	0.63	0.62	0.51	0.21	0.47	0.27
CO_2 removal ratio (%)		90.73	89.96	88.26	91.42	84.11	85.18	86.64
H_2S removal ratio (%)		92.34	90.24	90.36	91.95	96.46	92.68	95.49
Heat duty	Heater (kW)	885.56	536.98	696.89	716.91	5278.60	3242.67	3691.44
	Flash units (kW)	785.92	470.81	649.13	617.43	5341.35	3240.31	3639.91
	Pump (kW)	5.75	4.70	5.80	5.39	28.42	27.02	25.73
	Compressor (kW)	102.39	72.82	85.91	104.44	31.36	10.48	48.39
	In total (kW)	1779.62	1085.31	1437.73	1444.17	10679.73	6520.48	7405.47

Figure Captions

Figure 1 Proposed method for screening ILs as absorbents for simultaneous removal of CO_2 and H_2S from NG.

Figure 2 Flowsheet of the IL-based continuous acidic gas removal process.

Figure 3 *ASDI* of the involved cation-anion combinations for the individual (a) CO_2/CH_4 and (b) H_2S/CH_4 separation.

Figure 4 Comparison of the experimental and COSMO-SAC calculated VLE compositions for (a) {CO_2 + H_2S + [BMIM][$MeSO_4$]} and (b) {CO_2 + SO_2 + [HMIM][Tf_2N]} at around 296.00 K on IL-free basis.

Figure 5 Comparisons of *H*-based *ASDI* (red columns) and VLE-based *ASDI′* (blue columns) of the 29 prescreened ILs for (a) CO_2/CH_4 and (b) H_2S/CH_4 separation (Note: the ILs are arranged differently on the *x* axis in (a) and (b) for clear comparison).

Figure 6 VLE-based *ASDI′* for CO_2/CH_4 and H_2S/CH_4 of the 29 prescreened ILs.

Figure 7 Effect of the column height on (a) the mass purity and recovery of CH_4 and (b) the removal of CO_2 and H_2S.

Figure 8 Effect of the absorber pressure on (a) the mass purity and recovery of CH_4 and (b) the removal of CO_2 and H_2S.

Figure 9 Effect of the IL flow rate on (a) the mass purity and recovery of CH_4 and (b) the removal of CO_2 and H_2S.

Figure 10 Effect of the operating temperature and pressure of Flash-1 on (a) the CH_4 mass purity in the purified gas and (b) the CH_4 recovery.

Figure 11 Effect of the operating temperature and pressure of Flash-2 on (a) the CH_4 mass purity in the purified gas, (b) the CH_4 recovery and (c) the regenerated IL mass purity.

Figure 1

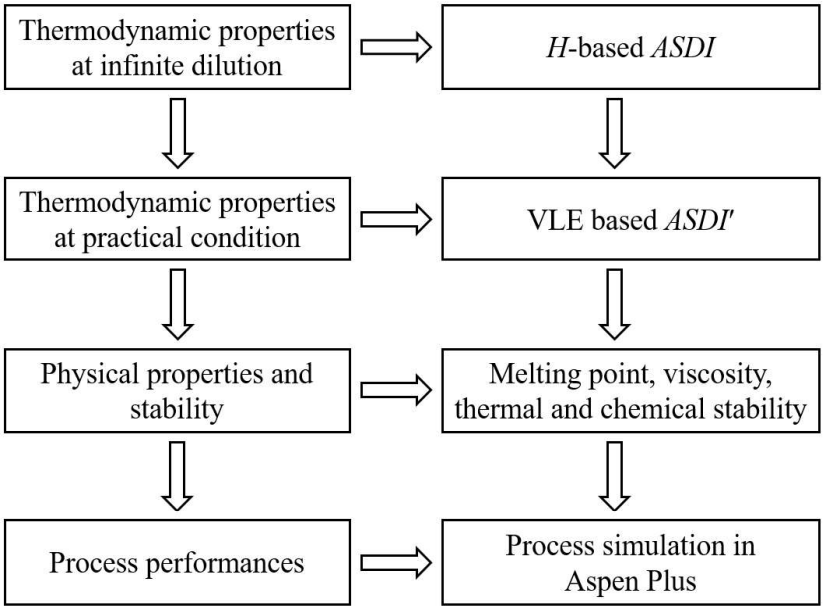
Thermodynamic properties at infinite dilution
H-based *ASDI*
Thermodynamic properties at practical condition
VLE based *ASDI'*
Physical properties and stability
Melting point, viscosity, thermal and chemical stability
Process performances
Process simulation in Aspen Plus

Figure 2

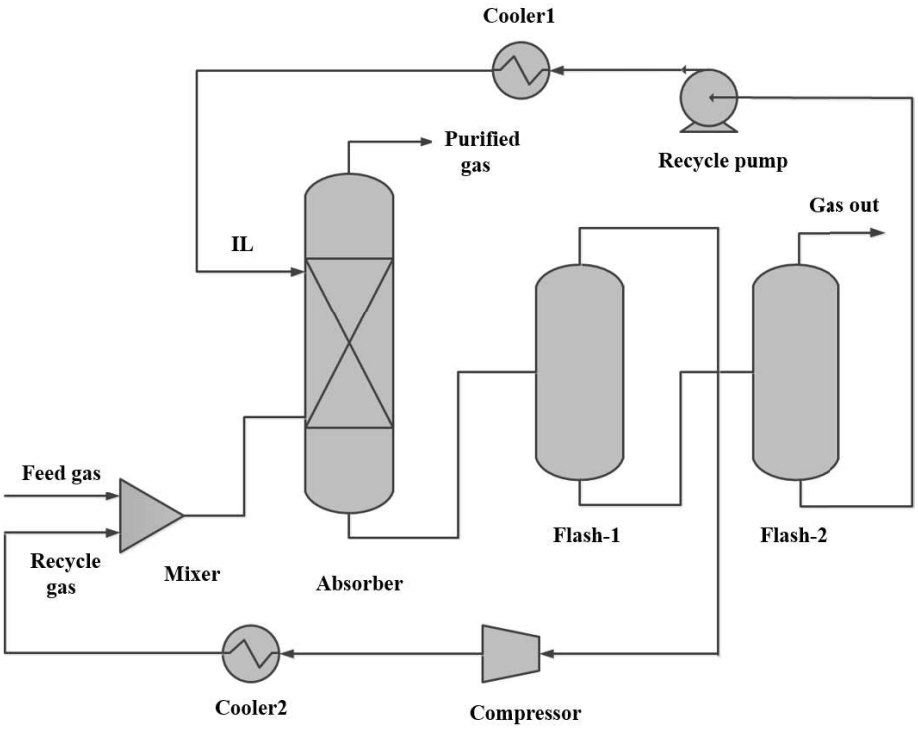
Cooler1
Purified gas
Recycle pump
Gas out
IL
Feed gas
Recycle gas
Mixer
Absorber
Flash-1
Flash-2
Cooler2
Compressor

Figure 3

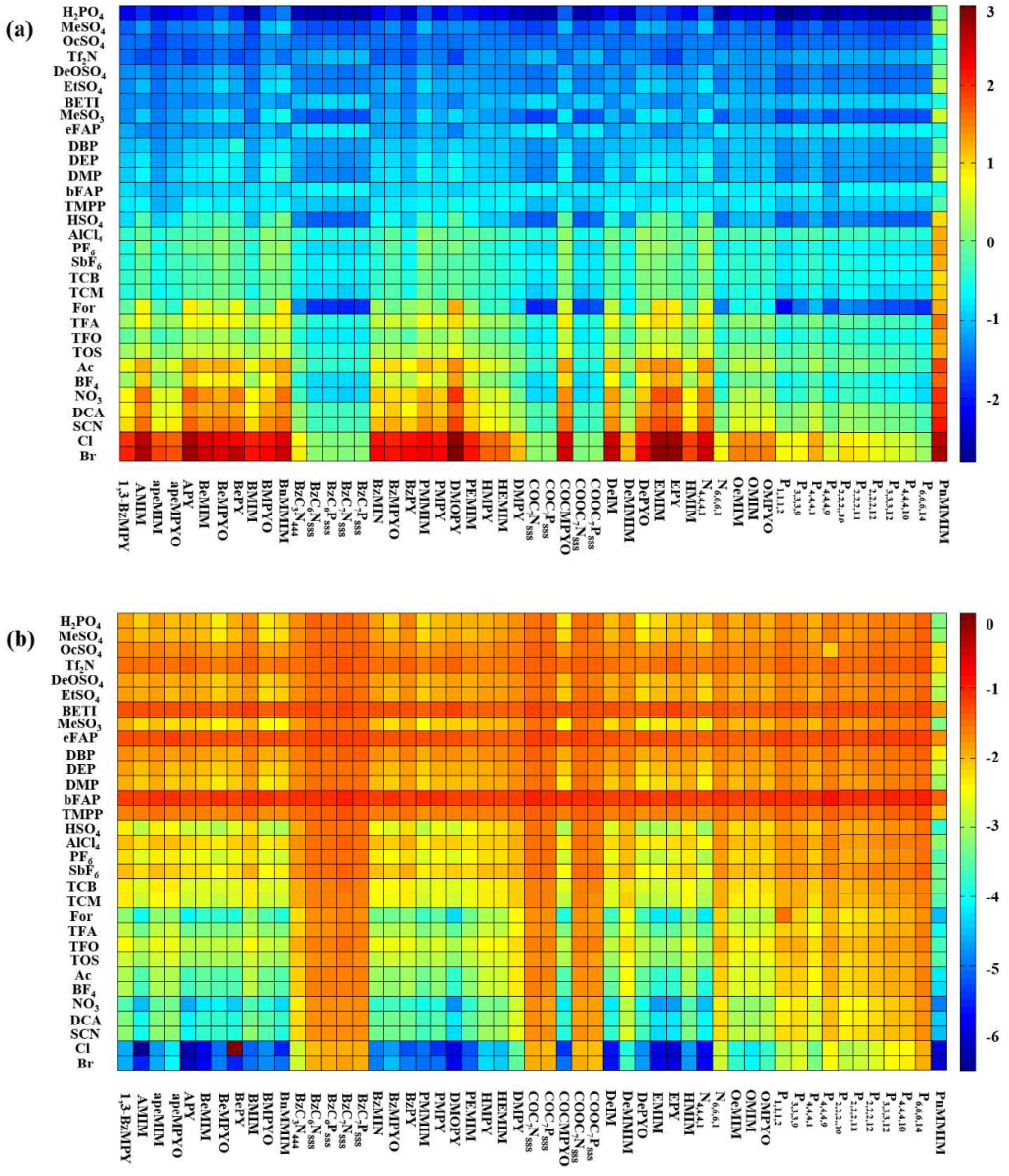
(a)
(b)
H_2PO_4
$MeSO_4$
$OcSO_4$
Tf_2N
$DeOSO_4$
$EtSO_4$
BETI
$MeSO_3$
eFAP
DBP
DEP
DMP
bFAP
TMPP
HSO_4
$AlCl_4$
PF_6
SbF_6
TCB
TCM
For
TFA
TFO
TOS
Ac
BF_4
NO_3
DCA
SCN
Cl
Br
1,3-BzMPY
AMIM
apeMIM
apeMPYO
APY
BeMIM
BeMPYO
BePY
BMIM
BMPYO
BnMMIM
BzC_3N_{444}
BzC_6N_{SSS}
BzC_6P_{SSS}
BzC_3N_{SSS}
BzC_3P_{SSS}
BzMIN
BzMPYO
BzPY
PMMIM
PMPY
DMOPY
PEMIM
HMPY
HEMIM
COC_3N_{SSS}
DMPY
COC_3P_{SSS}
COC_3NPYO
$COOC_3N_{SSS}$
$COOC_3P_{SSS}$
DeIM
DeMMIM
DePYO
EMIM
EPY
HMIM
$N_{4,4,4,1}$
$N_{6,6,6,1}$
OeMIM
OMIM
OMPYO
$P_{1,1,1,2}$
$P_{3,3,3,9}$
$P_{4,4,4,1}$
$P_{4,4,4,9}$
$P_{2,2,2,10}$
$P_{2,2,2,11}$
$P_{2,2,2,12}$
$P_{3,3,3,12}$
$P_{4,4,4,10}$
$P_{6,6,6,14}$
PnMMIM
3
2
1
0
-1
-2
-3
-4
-5
-6

Figure 4

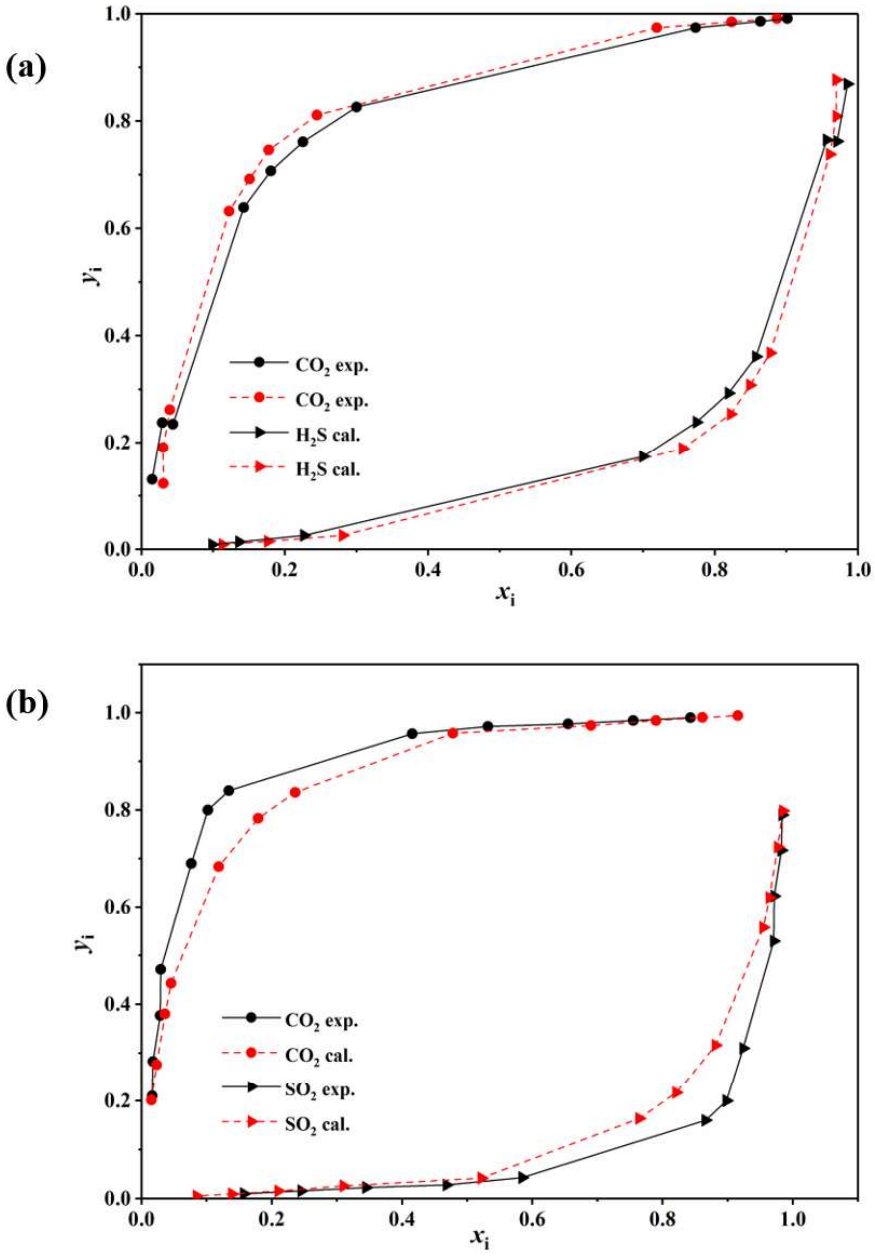
(a)
1.0
0.8
0.6
0.4
0.2
0.0
y_i
0.0
0.2
0.4
0.6
0.8
1.0
x_i
CO_2 exp.
CO_2 exp.
H_2S cal.
H_2S cal.
(b)
1.0
0.8
0.6
0.4
0.2
0.0
y_i
0.0
0.2
0.4
0.6
0.8
1.0
x_i
CO_2 exp.
CO_2 cal.
SO_2 exp.
SO_2 cal.

Figure 5

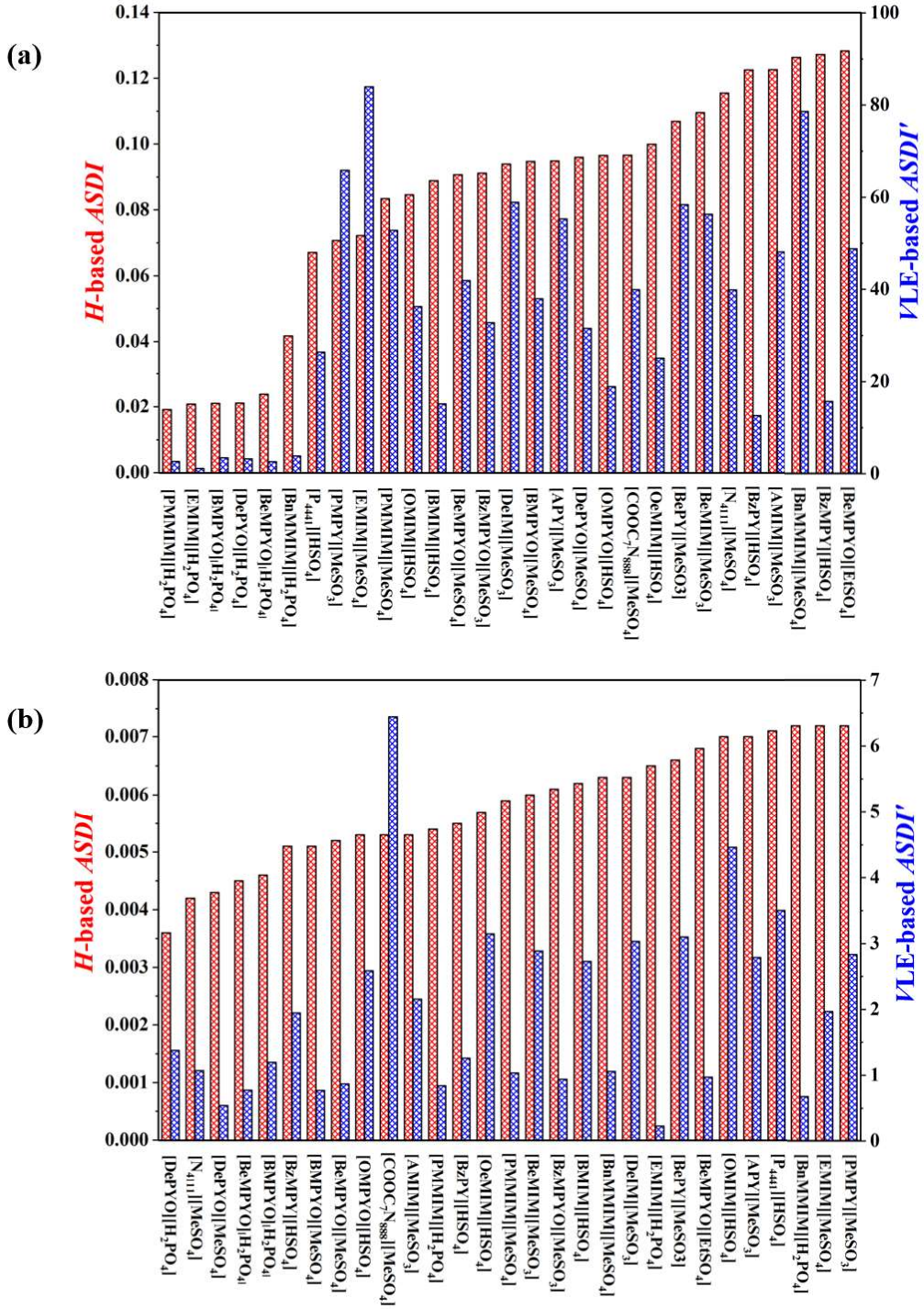
(a)
H-based ASDI
VLE-based ASDI'
0.14
0.12
0.10
0.08
0.06
0.04
0.02
0.00
100
80
60
40
20
0
[PMMIM][H2PO4]
[EMIM][H2PO4]
[BMPYO][H2PO4]
[DePYO][H2PO4]
[BeMPYO][H2PO4]
[BnMMIM][H2PO4]
[P444][HSO4]
[PMPY][MeSO3]
[EMIM][MeSO4]
[PMMIM][MeSO4]
[OMIM][HSO4]
[BMIM][HSO4]
[BeMPYO][MeSO4]
[BzMPYO][MeSO3]
[DeIM][MeSO4]
[BMPYO][MeSO4]
[APY][MeSO3]
[DePYO][MeSO4]
[OMPYO][HSO4]
[COOC-N8881][MeSO4]
[OeMIM][HSO4]
[BePY][MeSO3]
[BeMIM][MeSO4]
[N4111][MeSO4]
[BzPY][HSO4]
[AMIM][MeSO3]
[BnMMIM][MeSO4]
[BzMPY][HSO4]
[BeMPYO][EtSO4]
(b)
H-based ASDI
VLE-based ASDI'
0.008
0.007
0.006
0.005
0.004
0.003
0.002
0.001
0.000
7
6
5
4
3
2
1
0
[DePYO][H2PO4]
[N4111][MeSO4]
[DePYO][MeSO4]
[BeMPYO][H2PO4]
[BMPYO][H2PO4]
[BzMPY][HSO4]
[BMPYO][MeSO4]
[BeMPYO][MeSO4]
[OMPYO][HSO4]
[COOC-N8881][MeSO4]
[AMIM][MeSO3]
[PMMIM][H2PO4]
[BzPY][HSO4]
[OeMIM][HSO4]
[PMMIM][MeSO4]
[BeMIM][MeSO3]
[BzMPYO][MeSO3]
[BMIM][HSO4]
[BnMMIM][MeSO4]
[DeIM][MeSO4]
[EMIM][H2PO4]
[BePY][MeSO3]
[BeMPYO][EtSO4]
[OMIM][HSO4]
[APY][MeSO3]
[P444][HSO4]
[BnMMIM][H2PO4]
[EMIM][MeSO4]
[PMPY][MeSO3]

Figure 6

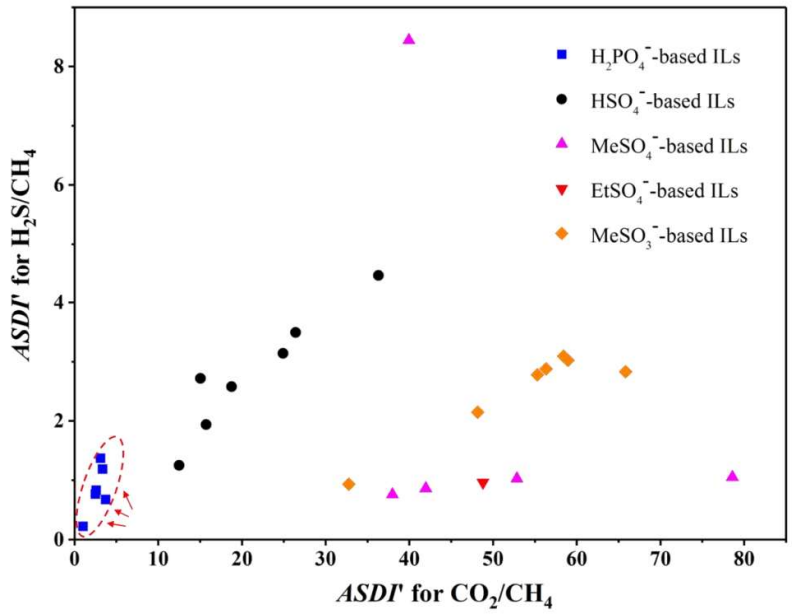
$H_2PO_4^-$-based ILs
HSO_4^--based ILs
$MeSO_4^-$-based ILs
$EtSO_4^-$-based ILs
$MeSO_3^-$-based ILs
ASDI' for H_2S/CH_4
ASDI' for CO_2/CH_4
0
2
4
6
8
0
10
20
30
40
50
60
70
80

Figure 7

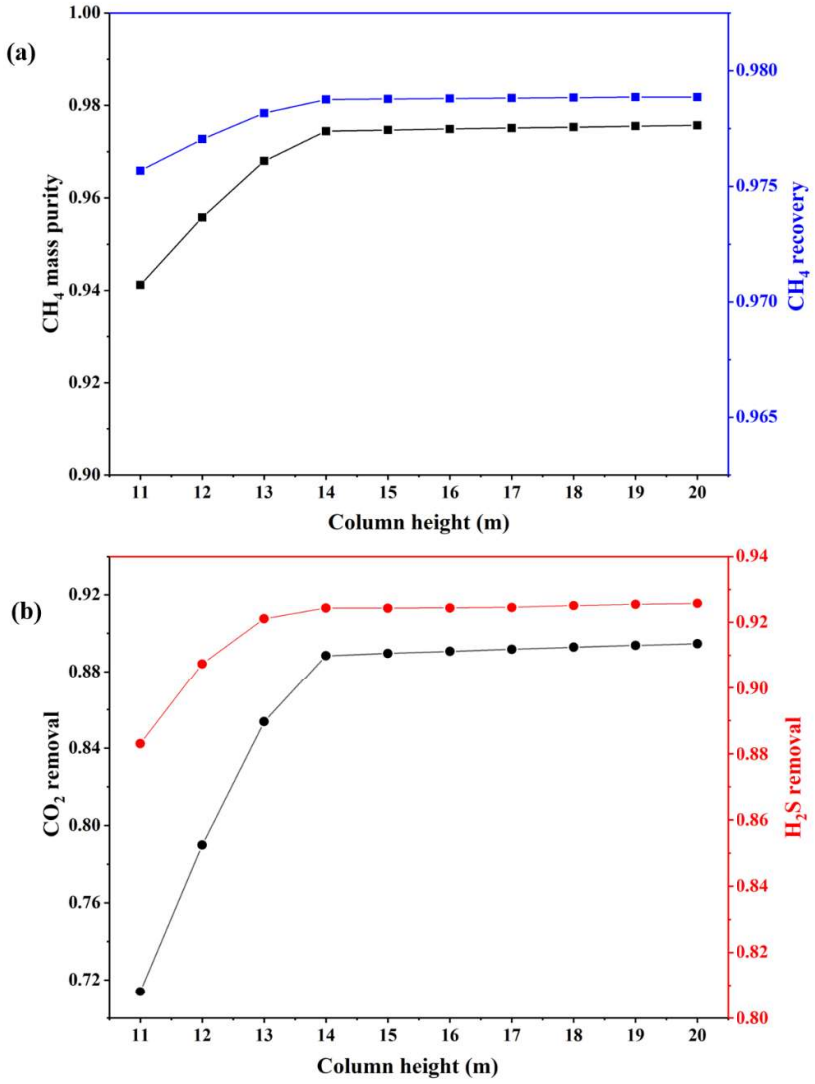
(a)
1.00
0.98
0.96
0.94
0.92
0.90
CH4 mass purity
0.980
0.975
0.970
0.965
CH4 recovery
11
12
13
14
15
16
17
18
19
20
Column height (m)
(b)
0.92
0.88
0.84
0.80
0.76
0.72
CO2 removal
0.94
0.92
0.90
0.88
0.86
0.84
0.82
0.80
H2S removal
11
12
13
14
15
16
17
18
19
20
Column height (m)

Figure 8

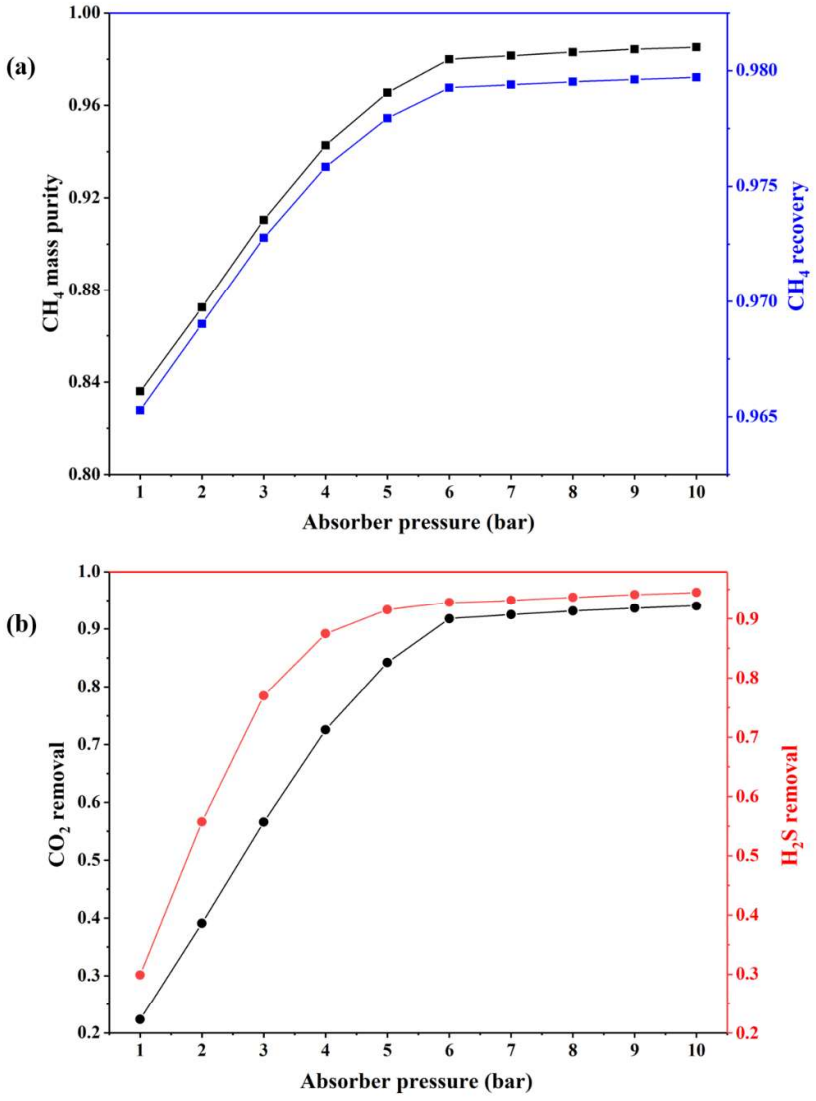
(a)
1.00
0.96
0.92
0.88
0.84
0.80
CH4 mass purity
0.980
0.975
0.970
0.965
CH4 recovery
1
2
3
4
5
6
7
8
9
10
Absorber pressure (bar)
(b)
1.0
0.9
0.8
0.7
0.6
0.5
0.4
0.3
0.2
CO2 removal
H2S removal
Absorber pressure (bar)

Figure 9

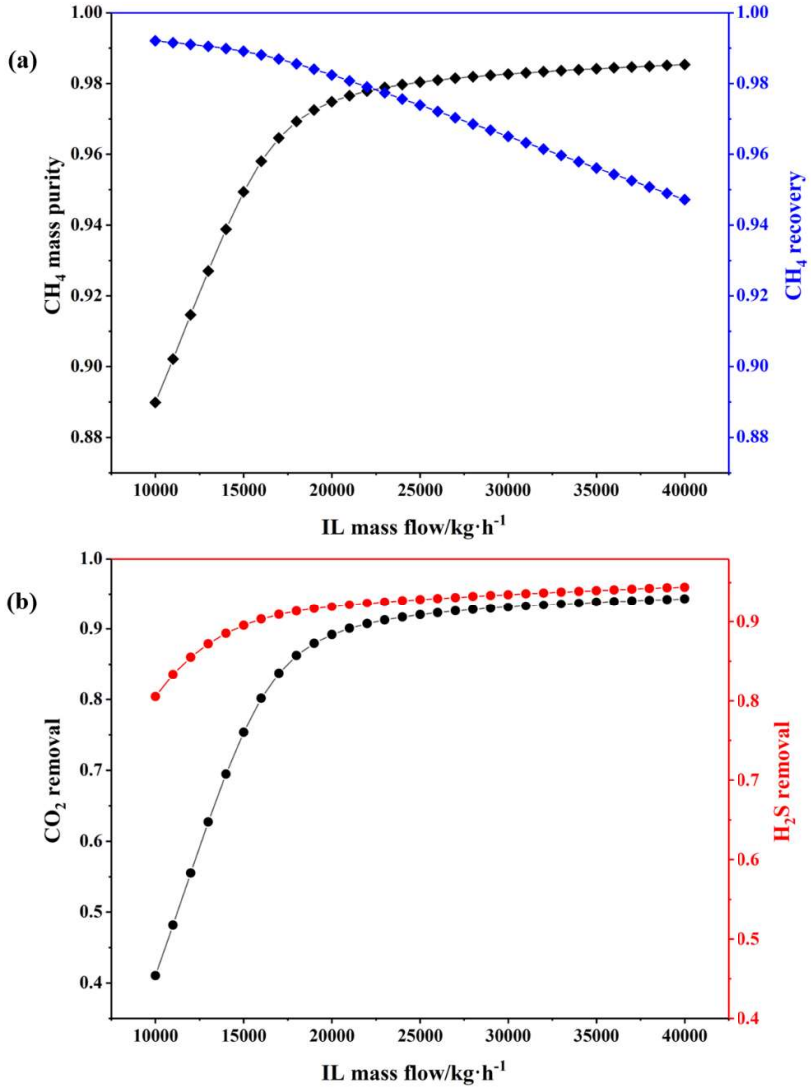
(a)
CH4 mass purity
CH4 recovery
IL mass flow/kg·h-1
(b)
CO2 removal
H2S removal
IL mass flow/kg·h-1

Figure 10

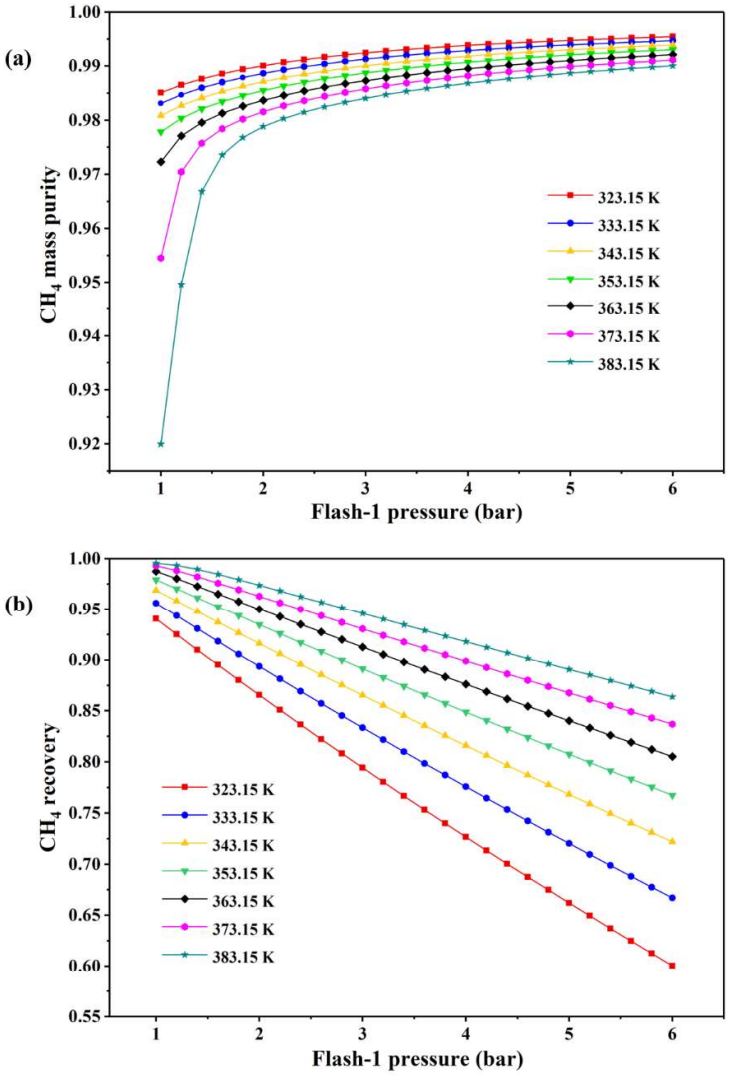
(a)
CH4 mass purity
Flash-1 pressure (bar)
323.15 K
333.15 K
343.15 K
353.15 K
363.15 K
373.15 K
383.15 K
(b)
CH4 recovery
Flash-1 pressure (bar)
323.15 K
333.15 K
343.15 K
353.15 K
363.15 K
373.15 K
383.15 K

Figure 11

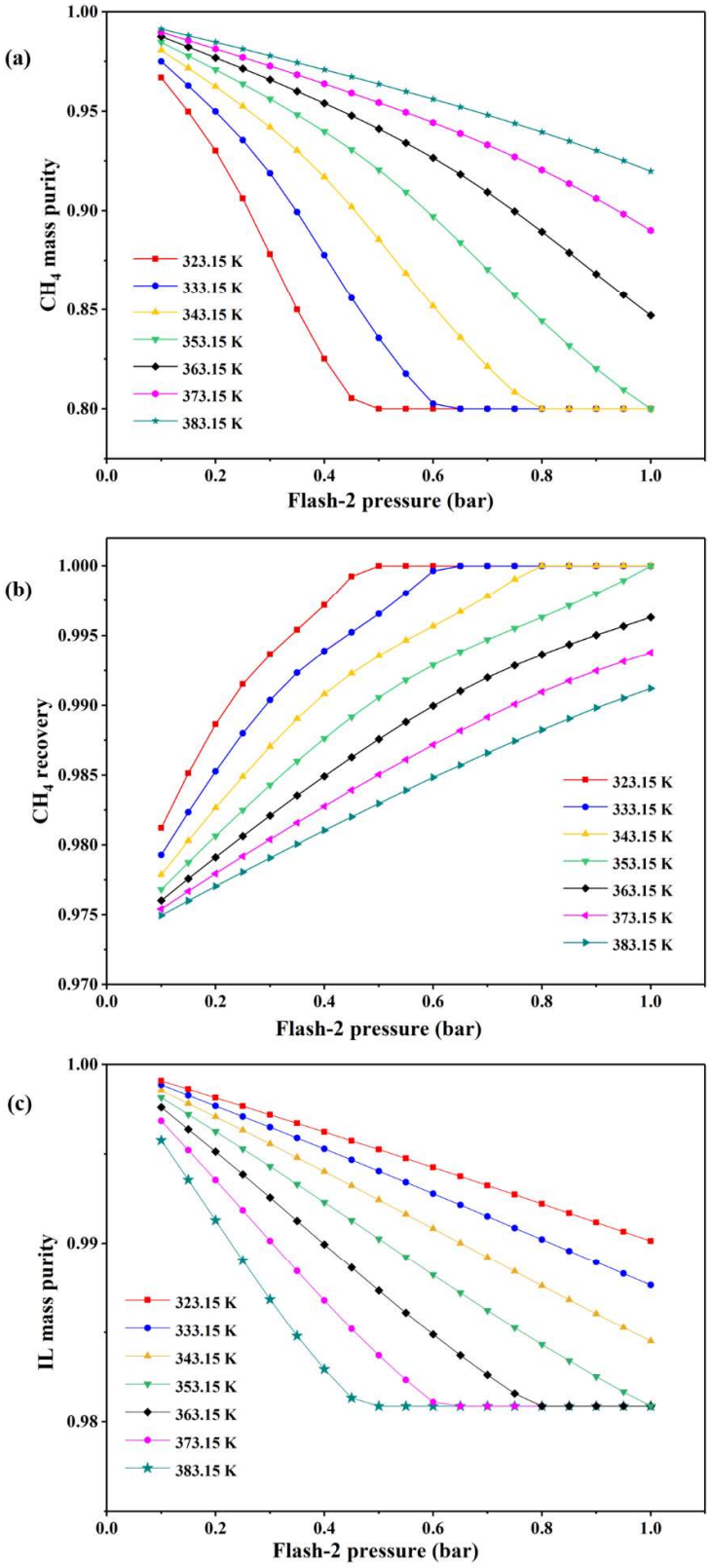
(a)
CH4 mass purity
Flash-2 pressure (bar)
323.15 K
333.15 K
343.15 K
353.15 K
363.15 K
373.15 K
383.15 K
(b)
CH4 recovery
Flash-2 pressure (bar)
(c)
IL mass purity
Flash-2 pressure (bar)